Nanotechnology

ACCEPTED MANUSCRIPT

Direct Large-Area Growth of Graphene on Silicon for Potential Ultra-Low-Friction Applications and Silicon-Based Technologies

Direct Large-Area Growth of Graphene on Silicon for Potential Ultra-Low-Friction Applications and Silicon-Based Technologies

Wei-Shiuan Tseng[1,2], Yen-Chun Chen[3], Chen-Chih Hsu[1], Chen-Hsuan Lu[4], Chih-I Wu[5], and Nai-Chang Yeh[1,*]

[1] Department of Physics, California Institute of Technology, Pasadena, CA, 91125, USA
[2] College of Photonics, National Chiao-Tung University, Hsin-Chu 30013, Taiwan
[3] Department of Physics, National Tsing-Hua University, Hsin-Chu 30013, Taiwan
[4] Department of Applied Physics and Materials Science, California Institute of Technology, Pasadena, CA 91125, USA
[5] Graduate Institute of Photonics and Optoelectronics and Department of Electrical Engineering, National Taiwan University, Taipei 106, Taiwan

E-mail: ncyeh@caltech.edu

Abstract

Deposition of layers of graphene on silicon has the potential for a wide range of optoelectronic and mechanical applications. However, direct growth of graphene on silicon has been difficult due to the inert, oxidized silicon surfaces. Transferring graphene from metallic growth substrates to silicon is not a good solution either, because most transfer methods involve multiple steps that often lead to polymer residues or degradation of sample quality. Here we report a single-step method for large-area direct growth of continuous horizontal graphene sheets and vertical graphene nano-walls on silicon substrates by plasma-enhanced chemical vapor deposition (PECVD) without active heating. Comprehensive studies utilizing Raman spectroscopy, X-ray/ultraviolet photoelectron spectroscopy (XPS/UPS), atomic force microscopy (AFM), scanning electron microscopy (SEM) and optical transmission are carried out to characterize the quality and properties of these samples. Data gathered by the residual gas analyzer (RGA) during the growth process further provide information about the synthesis mechanism. Additionally, ultra-low friction (with a frictional coefficient ~ 0.015) on multilayer graphene-covered silicon surface is achieved, which is approaching the superlubricity limit (for frictional coefficients < 0.01). Our growth method therefore opens up a new pathway towards scalable and direct integration of graphene into silicon technology for potential applications ranging from structural superlubricity to nanoelectronics, optoelectronics, and even the next-generation lithium-ion batteries.

Keywords: graphene-on-silicon, PECVD, AFM, superlubricity, XPS/UPS, RGA

1. Introduction

Graphene, a monolayer of carbon atoms forming a two-dimensional honeycomb structure, is known for its extraordinary electronic, optical, thermal, magnetic and mechanical properties [1−5]. Recently, several research groups have demonstrated that mesoscale graphite, which consists of many layers of graphene, offers superior properties as a solid lubricant that is promising for significantly reducing the wear and energy consumption in mechanical systems [6, 7]. The structural superlubricity of graphite may be attributed to the weak van der Waals (vdW) interaction of graphene

layers [8] with most materials and the lateral mechanical stiffness of graphite [9] when it forms incommensurable rigid crystalline contacts with most solid surfaces. Nevertheless, the aforementioned beneficial properties of graphite may not be realizable in the case of monolayer graphene because the morphology and characteristics of the substrate that supports the monolayer graphene will likely play a significant role in determining the friction between the monolayer graphene and other material surfaces [10,11]. Another major challenge associated with the realization of superlubricity is its scalability; superlubricity will cease to exist when the contact area scales up to the extent where disorder and imperfections become unavoidable. Thus, most superlubricity reported to date have only been achieved for submicron-scale contact areas [12,13].

A feasible approach to take advantage of the weak vdW interactions of graphene layers to achieve ultra-low friction for sliding on a variety of substrates is to deposit multilayer large-area graphene sheets on the substrates. Although the contact between the sliding object and multilayer graphene may not be as perfect as that on atomically flat monolayer graphene, any deformation from the surface corrugation of the underlying substrate can be considerably damped by the graphene layers if the thickness of multilayer graphene exceeds a characteristic penetration depth. This approach can therefore achieve an almost identical sliding condition on the very top layer of the graphene sheets independent of the substrate effects, which may serve as a promising solution for real-world applications.

However, a major challenge for using multilayer graphene as solid lubricant on substrates involves complicated and time-consuming transfer processes. The most common technique for transferring graphene from its growth substrate to a target substrate involves a polymer-supported method, which always leads to polymer residues on the transferred graphene surfaces and therefore degraded performance of the graphene-incorporated devices [14−17]. Other transfer methods without using polymers also involve multiple procedures such as copper etching, solution transfer, residue removal, and annealing [18−22], which generally lead to compromised graphene quality, including contaminations, damages, formation of wrinkles and bubbles, *etc*. Therefore, it is highly desirable to explore direct growth of graphene on common substrates, such as silicon, for better integration of graphene into existing industrial technology. In particular, direct growth of graphene on SiO_2/Si substrates can enable fully CMOS-compatible optoelectronic devices by exploitting various unique properties of graphene, including the high electron mobility, high modulation depth, large Kerr coefficient (~ 10^{10} -- 10^{13} m^2W^{-1}), low heat dissipation at GHz operation speeds, ultrafast photodetection, electrostatic gate-tunable broadband absorption and novel broadband photoluminescence [23-29], which are promising for the development of high performance photodetectors, optical modulators and hybrid optical interconnects.

To date, there have been few techniques developed for direct growth of graphene on silicon. Among the existing approaches, all of them require high-temperature (from 900 °C to 1550 °C) processing [30], and the resulting products are small graphene islands/flakes typically of sub-micrometer lateral scales [31−33]. In this work, we report the development of a new scalable method by means of plasma enhanced chemical vapor deposition (PECVD) to directly grow graphene with full coverage on large-area (~ 1 cm^2) substrates of silicon (Si), silicon dioxide (SiO_2), and diamond-like carbon (DLC) without the need of active heating. Systematic friction studies of graphene multilayers on Si substrates further indicate that ultra-low friction approaching the superlubricity limit has been achieved at micrometer scales. Given the importance of Si in modern technologies, our method of direct and scalable graphene growth on Si provides a pathway towards integrating graphene into Si-based technologies for applications ranging from structural superlubricity in nano/micro-electromechanical devices and hard drives [34], optoelectronic devices [23−28,35−42], to next-generation lithium-ion batteries [43−46].

2. Experimental

2.1 Graphene Synthesis

Figure S1 shows a schematic illustration of our PECVD system, which consists of a plasma source, a plasma cavity, a quartz growth tube, gases cylinders (containing CH_4, Ar and H_2), valves for mass flow control (MFC), vacuum gauges, and vacuum pumps. Immediately before placing silicon substrates into the processing tube, we used hydrofluoric acid (HF) to etch away the native oxides on the substrate surface (for around 20 minutes) to ensure that most of the oxides were removed. This step helped temporarily passivate the reactive silicon surface by forming silicon-hydrogen bonds on the substrate surface to minimize surface oxidation. Before turning on the plasma, we introduced all necessary gases into the tube at the same time and reached the desired partial pressures for all gases by using the MFCs to control the gas flow rates. When all gas flows reached a steady state, the plasma source was turned on to ionize gas molecules into energetic ions and radicals to induce reactions with the substrate.

For this single-step PECVD growth process, the type of final graphene products is determined by three critical parameters: the ratio of methane-to-hydrogen flow rates, the plasma power, and the growth time. In this study, the plasma power was fixed at ~ 70 Watts over ~ 1 cm^3 volume and the growth time required was 10 minutes. By controlling the methane and hydrogen rates, we could fabricate either

horizontal graphene sheets or vertical graphene nano-walls. Specifically, when the ratio of CH_4-to-H_2 flow rates was less than 5.5, we usually obtained horizontal graphene sheets on the silicon surface. On the other hand, vertical graphene nano-walls could be synthesized by controlling the ratio of CH_4 to H_2 gas flows to a value greater than 5.5.

2.2 Characterization

Raman spectra were obtained via a Renishaw M1000 micro-Raman spectrometer system using a 514.3 nm laser (2.41 eV) as the excitation laser source. SEM images were taken using FEI Nova 600 NanoLab. Studies of the x-ray photoelectron spectroscopy (XPS) and ultraviolet photoelectron spectroscopy (UPS) were carried out via the Kratos-Ultra-XPS model, which employed a magnetic immersion lens with a spherical mirror and concentric hemispherical analyzers with a delay-line detector for both imaging and spectroscopy. The UPS were measured via He I (21.2 eV) as the excitation source under a base pressure of $\sim 10^{-10}$ Torr. Photoelectrons emitted from the sample were recorded by a hemispherical analyzer with an overall resolution of 0.05 eV, as determined from the width of the Fermi step measured on a gold substrate cleaned by Ar ion sputter. The vacuum levels of the samples were derived from the secondary-electron cutoff of the UPS spectra at the high binding energy sides. The energy difference between the secondary-electron cutoff and the Fermi level on the spectra was obtained as the value of the work function.

Al Kα (1.486 keV) monochromatic X-rays and He I (21.2 eV) were used as the excitation sources for XPS and UPS measurements, respectively, in an ultrahigh vacuum chamber with a base pressure lower than 2×10^{-10} Torr. Optical transmission spectra were collected using a Cary 5000 absorption spectrometer with an integrating sphere, and quartz substrates were used for the samples. The procedure for preparing graphene samples for the optical measurement involved the following steps: First, the graphene-covered Si substrate was placed into a Teflon beaker filled with buffered oxide etch (BOE). The Si substrate remained afloat on the liquid due to surface tension. After at least 24 hours, the surface oxide between graphene and Si was fully etched away so that the graphene sample was freed from the substrate and suspended on the liquid surface. Here we note that the typical substrates used for these experiments were $\sim (0.5 \text{ cm} \times 0.5 \text{ cm})$ in dimension, which was sufficiently small to ensure fast exfoliation. Next, the liquid-exfoliated graphene samples were scooped off from the liquid surface and transferred to another beaker filled with DI water to rinse off the residual BOE. This process was repeated several times to ensure that the graphene was completely free of chemical residues. A quartz substrate was then inserted to the bottom of the beaker, and DI water was slowly drained until graphene landed on top of the substrate. Finally, a 15-minute mild annealing of the graphene

sample on quartz substrate was carried out to remove residual DI water.

AFM images and friction measurements were performed on a Bruker Dimension Icon AFM. Two modes of AFM were used: the tapping mode and the contact mode. The tapping mode was used to acquire the surface morphology and the contact mode was used to analyze the frictional force. For the friction measurements, a triangular cantilever made of SiN and coated with reflective gold (Bruker DNP-10) was used for the lateral force microscopy (LFM) tests. The thickness, length, width, and spring constant of the cantilever were 0.6 μm, 205 μm, 25 μm, and 0.06 N/m, respectively. The height and radius of the tip on the cantilever were 5.5 μm and 20 nm, respectively. To extract the applied normal force from the voltage signal of the AFM system, the following formula was used: Normal force (N) = [voltage (V)] × [deflection sensitivity (nm/V)] × [spring constant (N/m)]. The deflection sensitivity was calibrated every time by doing a force-curve scan before the friction measurements. To convert the measured voltage signal to the friction force, the following formula was applied [47]:

$$f = \frac{0.4 h K_L V}{L\, S_{Dif}}$$

Here h is the height of the tip, L is the length of the cantilever, V is the measured voltage signal, S_{Dif} is the deflection sensitivity, and the K_L is given by the following expression:

$$K_L = \frac{GWt^3}{3L}\left(\frac{1}{h + t/2}\right)^2$$

where G is the shear modulus (= 1.69×10^{11} Pa), W is the width of the cantilever, and t is the thickness of the cantilever.

3. Results and discussion

3.1 Characterization of PECVD-grown Graphene Sheets on Silicon

In figure 1(a) we show a representative scanning electron microscopy (SEM) image of as-grown graphene sheets fully covering the underlying Si substrate after only 10 minutes of PECVD growth. Details of the synthesis conditions are described in the Experimental section, and experimental setup of the PECVD system has been reported previously [48, 49]. The SEM image indicates that the as-grown graphene layers generally exhibit multi-domain distributions with varying thicknesses. The lateral dimension of each graphene layer is typically much larger than 1 μm although it is difficult to identify the borders associated with individual sheets because they mostly overlap each other.

To characterize the quality of the graphene multilayers on Si, we performed Raman spectroscopic studies on various random areas of each sample and found consistent spectra throughout, implying uniform quality of the as-grown

graphene multilayers on Si. As shown in figure 1(b), the representative Raman spectrum taken on a sample of multilayer graphene-on-Si reveals typical graphene Raman modes of the 2D, G- and D-bands with narrow FWHM [50, 51]. The intensity of the 2D-band at (2696 ± 2) cm^{-1} in the Raman spectrum was larger than that of the G-band at (1583 ± 2) cm^{-1}, and an intense D-band was also observed due to the presence of many boundaries around the edges of graphene sheets, which was further accompanied by the D′-band at (1615 ± 2) cm^{-1} as the result of an intense D-band. The optical micrographs shown in the inset of figure 1(b) were taken on a $(1$ cm $\times 1$ cm$)$ area of a Si substrate before and after the PECVD graphene growth. Evidently the Si substrate after graphene growth was still somewhat reflective, which

indicated that the graphene layers on Si were relatively thin and semi-transparent.

Additional characterizations of the physical and chemical properties of the graphene-covered Si samples were investigated by X-ray and ultraviolet photoemission spectroscopy (XPS and UPS). The XPS spectrum in figure 1(c) revealed a clean sample surface with only C-1s and O-1s signals. The dominant C-1s peak $(> 95\%)$ was from the as-grown graphene multilayers, whereas the presence of a small O-1s peak $(< 5\%)$ may be attributed to broken Si-O bonds from the substrate surface, which will be further elaborated in the context of the growth mechanism later. In particular, we note that no Si peaks could be found in the XPS spectrum, which implied a full coverage of graphene on the Si substrate
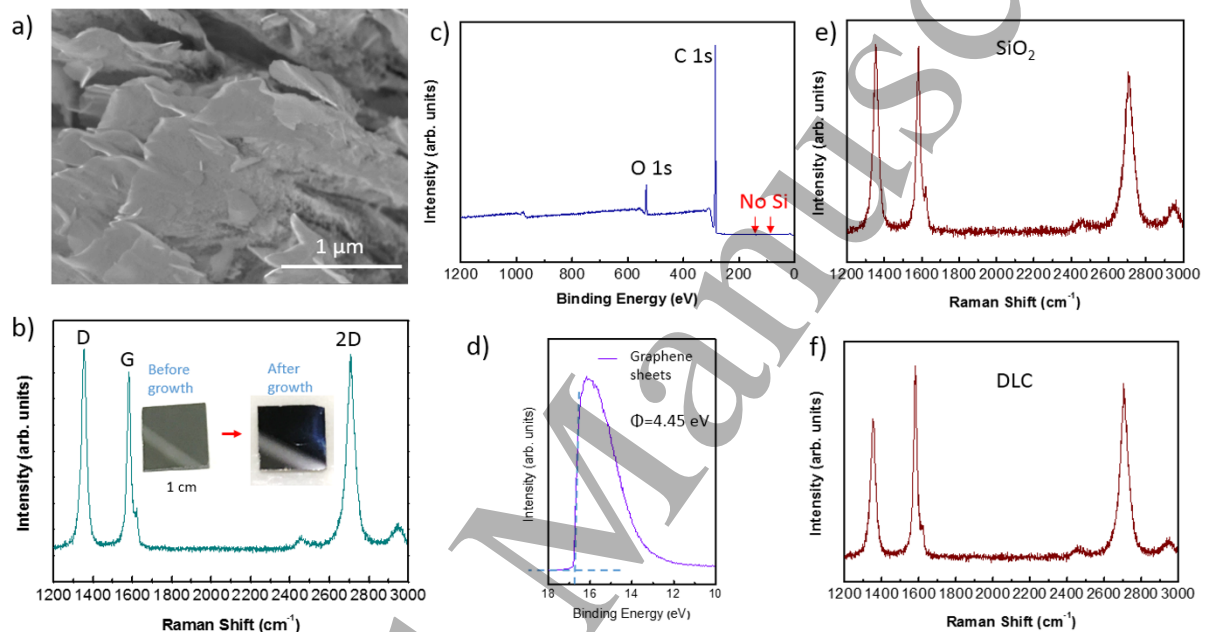

Figure 1. (a) SEM image taken on an as-grown sample of multilayer graphene fully covering a Si substrate. The sample were synthesized with the following growth parameters: applied plasma power, 70 Watts; plasma volume, ~ 1 cm^3; growth time, 10 minutes; and ratio of CH$_4$-to-H$_2$ flow rates, < 5.5. (b) Main panel: Raman spectrum of the sample shown in (a), revealing typical Raman modes of graphene with the 2D-, G- and D-bands. The inset are optical micrographs of the substrate before and after graphene growth. (c) XPS analysis of the as-grown graphene-on-Si sample, showing a dominant C-1s $(> 95\%)$ peak and a secondary O-1s $(< 5\%)$ peak. The complete absence of any Si peaks implied full graphene coverage on the Si substrate. (d) UPS spectrum of the as-grown graphene-on-Si sample, showing a work function (4.45 ± 0.05) eV consistent with that of pristine graphene without doping. (e)-(f) Raman spectra of as-grown graphene sheets on (e) SiO$_2$ and (f) diamond-like carbon (DLC) substrates, respectively. Both spectra reveal distinct D, G and 2D bands of graphene Raman modes with slightly different D-band intensities and 2D/G ratios.

and also corroborated the finding from the SEM image in figure 1(a). The work function of the graphene layers was also examined through UPS and the result was shown in figure 1(d). The value deduced from the secondary electron cutoff of the UPS spectrum was (4.45 ± 0.05) eV, which was in good agreement with the typical value of pristine graphene without doping. Direct PECVD growth of graphene on SiO$_2$ and DLC

substrates was also achieved with slightly different growth parameters, as shown in figure 1(e) and 1(f). These results suggest that our PECVD growth method is a universal and scalable technique for depositing graphene on a wide variety of substrates ranging from metallic to insulating materials. In this work we mainly focus on the studies of graphene grown on Si because of the broad range of Si-based applications.

3.2 Morphology and Thickness Studies

To investigate the surface morphology and thickness of the as-grown graphene layers on Si, tapping mode atomic force microscopy (AFM) was conducted on a Si substrate both before and after graphene growth. Figure 2(a) shows a high-sensor AFM image of the graphene-covered Si surface, which revealed multiple domains with varying heights throughout the micrometer-scale area. The layered structures on the surface were the as-grown graphene sheets with an averaged lateral dimension larger than 1 μm. The thickness of the sheets

was examined by studying the cross-sectional profiles. As the cross-sectional profiles revealed in the lower panels of figure 2(a), we observed different steps along lines a, b, and c. The cross-section along line a showed a 1.4 nm step that corresponded to 4 layers of graphene, whereas that along line b revealed a 0.7 nm step that corresponded to two layers of graphene thickness. These results suggested that the surface consisted of integer numbers of graphene layers within the resolution of the AFM [52, 53], which were also in agreement with the SEM image shown in figure 1. More importantly, we note that along line c in figure 2(a), the absence of any
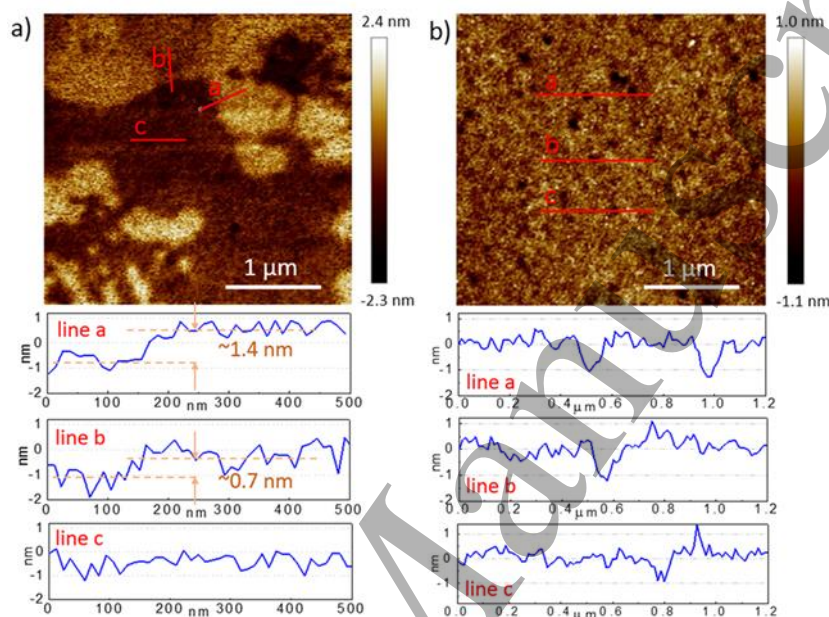

Figure 2. (a) AFM image and cross-sectional profiles of a fully graphene-covered Si surface. Here the growth parameters for the sample were: applied plasma power, 70 Watts; plasma volume, ~ 1 cm^3; growth time, 10 minutes; ratio of CH_4-to-H_2 flow rates, < 5.5. (b) AFM image and cross-sectional profiles of a bare Si (100) surface.

discernible height variations within instrumentation resolution suggested that the profile was taken on an atomically flat surface. We note that such atomically flat regions were found to have a lateral dimension larger than a few to tens of micrometers, suggesting that the individual graphene layers grown on Si by the PECVD method were several orders of magnitude larger than the sub-micrometer scale flakes obtained by others in the past [31–33].

In addition to understanding the surface topography of graphene-covered Si substrate, we performed the same studies on bare Si surface as a reference for comparison, and the results are shown in figure 2(b). From the cross-sectional profiles, we found that the roughness of the Si surface was mostly within 1 nm. However, a few pits along lines a and b with depths larger than 1 nm were found, as shown in the lower panels of figure 2(b). Additionally, sharp particles with heights taller than 1 nm were observed along lines b and c in

the cross-sectional profiles. Combining the findings from figure 2(a) and 2(b), we suggest that the as-grown graphene layers can effectively smooth out small pinholes and deposits on the Si surface, resulting in reduced roughness as exemplified by the relatively flat morphology along line c on the graphene-covered surface. The reduction of surface roughness can contribute to lower sliding friction, which has been independently verified by studies of the friction and will be discussed in the last part of this paper.

3.3 Synthesis and Characterization of Graphene Nano-Walls

In general, the growth conditions inside the PECVD chamber can be modified significantly through varying the plasma power, growth time, and methane (CH_4) to hydrogen (H_2) ratio. This flexibility led to the successful synthesis of vertical

graphene nano-walls directly on Si surface by increasing both the plasma power and the ratio of CH_4/H_2 partial pressures. Figure 3(a) shows a representative SEM image of graphene nano-walls fully covering the surface of a Si substrate after 10 minutes of PECVD growth process. The vertical graphene nano-walls appeared to distribute uniformly over the entire (1 cm × 1 cm) Si substrate, although their surface morphology was totally different from the horizontal graphene sheets shown in figure 1(a). The full coverage of graphene nano-walls was further confirmed by the optical micrographs shown in figure 3(b). After 10 minutes of graphene growth, the Si substrate revealed a totally darkened surface without any metallic reflection, indicating that graphene had fully covered the entire surface of the Si substrate. Here we remark that the distinctly different optical properties of graphene nano-walls

from graphene sheets may be attributed to combined effects of different geometries and a substantial vertical height of graphene nano-walls that led to significant sub-wavelength photon scattering and trapping [54].

To determine the height of the graphene nano-walls, the tapping mode AFM was no longer suitable because the rapid height variations were too much for delicate AFM tips. Therefore, we resorted to enlarging and tilting the SEM images at 15° to estimate the height of the nano-walls. As shown in figure 3(c), the average height of these graphene nano-walls was ~ 300 nm whereas the typical thickness of the nano-walls was 10 ~ 30 nm, corresponding to a few tens of stacked graphene layers. These findings were similar to the typical height and thickness of graphene nanostripes (GNSPs)
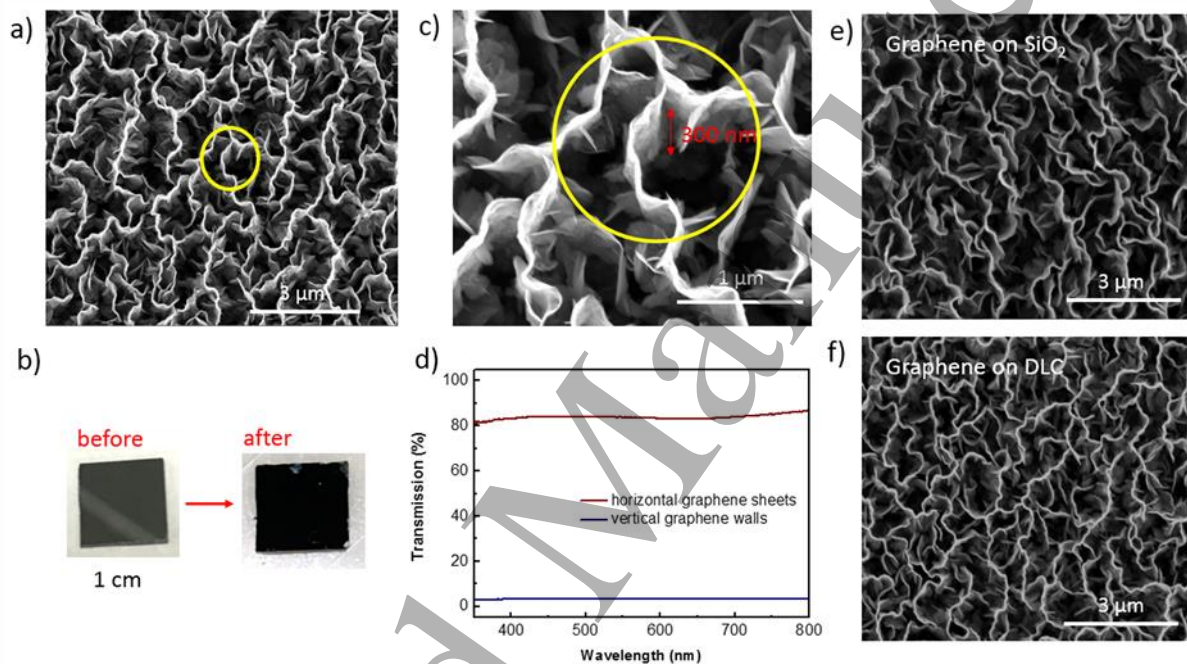

Figure 3. (a) SEM image of the sample surface with full coverage of graphene nano-walls on Si after 10 minutes PECVD process. (b) Optical micrographs of Si substrates before and after the growth of graphene nano-walls. The growth parameters for this sample were: applied plasma power, 70 Watts; plasma volume, ~ 1 cm³; growth time, 10 minutes; ratio of CH_4-to-H_2 flow rates, > 5.5. (c) SEM image enlarged from (a) and tilted at 15°, showing a mostly consistent graphene nano-wall height of ~ 300 nm. (d) Comparison of the optical transmission spectra of horizontal graphene sheets and vertical graphene nano-walls grown on Si and transferred to quartz substrates. (e)-(f) SEM images of graphene nano-walls grown on (e) SiO_2 and (f) DLC substrates, respectively. The growth parameters for graphene synthesis on SiO_2 and DLC were consistent with those used for synthesis of graphene nano-walls on Si.

grown on copper substrates by PECVD, although the length-to-width aspect ratios of GNSPs after exfoliation were approximately one order of magnitude larger than those of the nano-walls [55]. Additionally, optical transmission studies were carried out by transferring graphene nano-walls from Si onto quartz substrates and then compared with the results from horizontal graphene sheets similarly transferred from Si to

quartz substrates, as shown in figure 3(d). The transferred graphene sheets revealed a transmission percentage more than 80% across the visible light range, indicating an average thickness less than 7 layers [56]. In contrast, < 2% optical transmission was observed from 350 nm to 800 nm for the transferred graphene nano-walls (figure 3(d)), which was consistent with the completely darkened surface of the sample

fully covered by graphene nano-walls (figure 3(b)). The vanishing optical transmission may be attributed to multiple sub-wavelength scattering and effective light trapping in these quasi-one-dimensional graphene nanostructures as well as light absorption by the gapless graphene nano-walls [48, 54].

The chemical and electronic characteristics of graphene nano-walls grown on Si were also investigated using XPS/UPS, which yielded results similar to those obtained from the graphene sheets grown on Si, as illustrated in figure S2. Additionally, we successfully carried out direct-growth of graphene nano-walls on DLC and SiO_2 without metal catalysis, and the corresponding SEM images are shown in figure 3(e) and 3(f).

3.4 Discussion: Plasma Effects and Growth Mechanism

Based on the aforementioned experimental results and data obtained from the residual gas analyzer (RGA), we conjecture the following growth mechanism of graphene on Si by considering the nucleation processes and plasma effects.

Figure 4(a) illustrates the initial condition before igniting the plasma source: The growth chamber was firstly filled with CH_4 and H_2, whereas the Si surface was covered by some native oxide together with hydrogen-terminated Si bonds – Although we had applied hydrofluoric acid (HF) to remove the surface SiO_2 and to passivate the surface of the Si substrate by hydrogen immediately before inserting the Si substrate into the growth tube, it was inevitable to still have some degrees of native oxide formation. After the plasma was turned on, both the surface Si-O and Si-H bonds as well as the C-H bonds in methane were broken by energetic radicals in the plasma so that most of the oxygen atoms reacted with carbon atoms and formed carbon monoxide, as schematically illustrated in figure 4(b) and empirically verified by the RGA record (see figure 4(g)) that indicated a notable increase of CO after the plasma was turned on (dark-red arrow). Similar studies were also conducted on the PECVD growth of graphene on SiO_2 substrates, which revealed even stronger CO signals from the RGA as shown in figure S3(a) and further confirmed the notion that surface oxides were removed by plasma during the
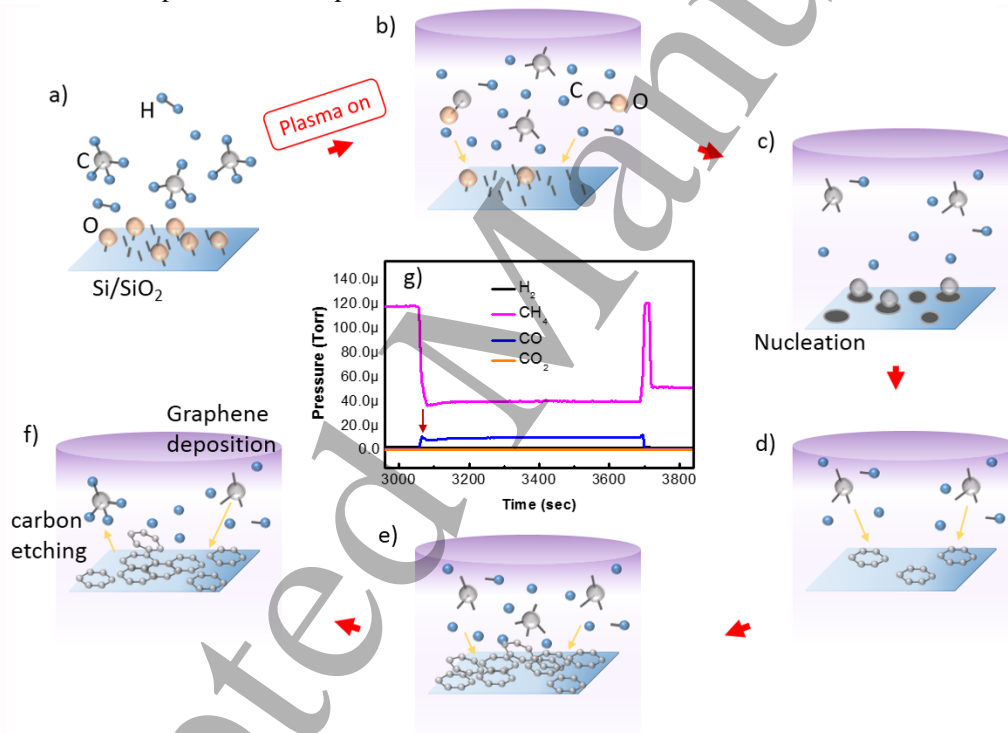

Figure 4. (a) Initial environment inside the growth chamber filled with CH_4, H_2, and also some native SiO_2 on the Si surface. (b) Plasma ignition. Carbon and oxygen started to disassociate from CH_4 and Si, respectively. (c) Formation of carbon nucleation sites on Si surface. (d) Ensuing graphene growth from continuous CH_4 supply. (e) The formation of stacking graphene sheets or vertical graphene nano-walls under sufficiently high plasma power and excess carbon supply. (f) Two competing dynamic processes: graphene deposition and carbon etching. (g) RGA record of different gases in the growth chamber over 10 minutes time period.

growth process. For both Si and SiO_2 substrates, we note that the increase of CO_2 was far less than CO, which may be attributed to the limited surface native oxides, although the elevation of CO_2 signal for the PECVD growth of graphene on

SiO_2 substrates after igniting plasma was still higher than that for the growth on Si substrates due to more surface oxides in the former, as shown in figure S3(b).

The removal of surface Si-O and Si-H bonds resulted in many surface Si dangling bonds, which were highly reactive and so could snatch carbon atoms in the plasma to nucleate graphene growth on Si surface, as depicted in figure 4(c). This scenario is consistent with the precipitous drop of CH_4 pressure in the RGA spectra upon igniting the plasma. Continuous CH_4 supply together with active carbon decomposition and reactive Si surface dangling bonds contributed to the ensuing growth of graphene along the in-plane direction from various nucleation centers and eventually covered the entire substrate, as schematically shown in figure 4(d) and 4(e). With continuing growth time, new graphene sheets began to develop from the Si surface due to the relatively weak interaction between graphene and Si, which elevated the already grown graphene sheets and stacked into multilayers.

Interestingly, we found that for sufficiently high plasma power and CH_4 supply, vertical graphene nano-walls rather than horizontal graphene sheets would predominantly grow from Si. We conjecture that in addition to the removal of surface Si-O and Si-H bonds, highly energetic radicals in the plasma could create numerous small craters on the surface of Si substrate, which may favor vertical growth of graphene nano-walls from the craters in the presence of excess free carbon atoms. This is because the creation of craters results in local curvatures on the substrate surface, which tend to promote the randomness of nucleated nano-graphene and limit substantial extension of horizontal graphene growth, particularly in the presence of excess carbon source when anisotropic growth along the vertical direction is strongly enhanced.

During the PECVD growth processes, the in-plane propagation of graphene growth could always be terminated by the formation of C–H bonds and/or carbon etching by energetic radicals in the hydrogen plasma. Therefore, as shown in figure 4(f), proper control of the CH_4/H_2 ratio to balance the two dynamic processes of graphene deposition and carbon etching plays a crucial role in this PECVD growth of

graphene. Additionally, the presence of energetic radicals to remove surface oxides from Si and to extract carbon from CH_4 during the PECVD growth process is the key factor that makes the deposition of graphene on Si much easier than the thermal CVD methods.

3.5 Studies of the Sliding Friction on Graphene-Covered Silicon Surfaces

To understand the effect of graphene layers on the sliding friction of graphene-covered Si surface, we used the lateral force microscopy (LFM) of the contact-mode AFM to conduct surface friction studies as a function of the graphene thickness, applied normal force, and contact area. Only horizontal graphene sheets were investigated because vertical graphene nano-walls were not expected to reduce surface frictions effectively. To determine the number of graphene layers, we first estimated it by the intensity ratio of the 2D-to-G Raman modes, and then conducted cross-sectional AFM measurements to obtain a more accurate value as shown in figure S4. Two thicknesses of graphene sheets with averaged values of 0.9 nm and 5 nm were investigated systematically, which corresponded to approximately 3 and 14 layers of graphene, respectively, given the resolution of AFM.

Figure 5(a) shows the measured friction between the AFM tip and sample surface as a function of applied normal forces averaged over a (300 nm × 300 nm) area. Without graphene coverage, the bare Si surface exhibited a relatively low friction under a small normal force of 12.96 nN, but the friction increased rapidly when the normal force reached 19.44 nN. The dependence of friction on the normal force became very different for graphene-covered Si surfaces: Despite slightly larger frictions under smaller loads, both graphene-covered samples exhibited much smaller increase in friction with the increasing load than the bare Si surface. In particular, the Si surface covered with 14 layers of graphene revealed the lowest friction for a normal force of 19.44 nN or larger, as shown in figure 5(a). This finding suggests that a sufficiently large number of graphene layers on top of a substrate can mitigate the surface roughness effect of the underlying substrate, leading to significant reduction in the sliding friction.
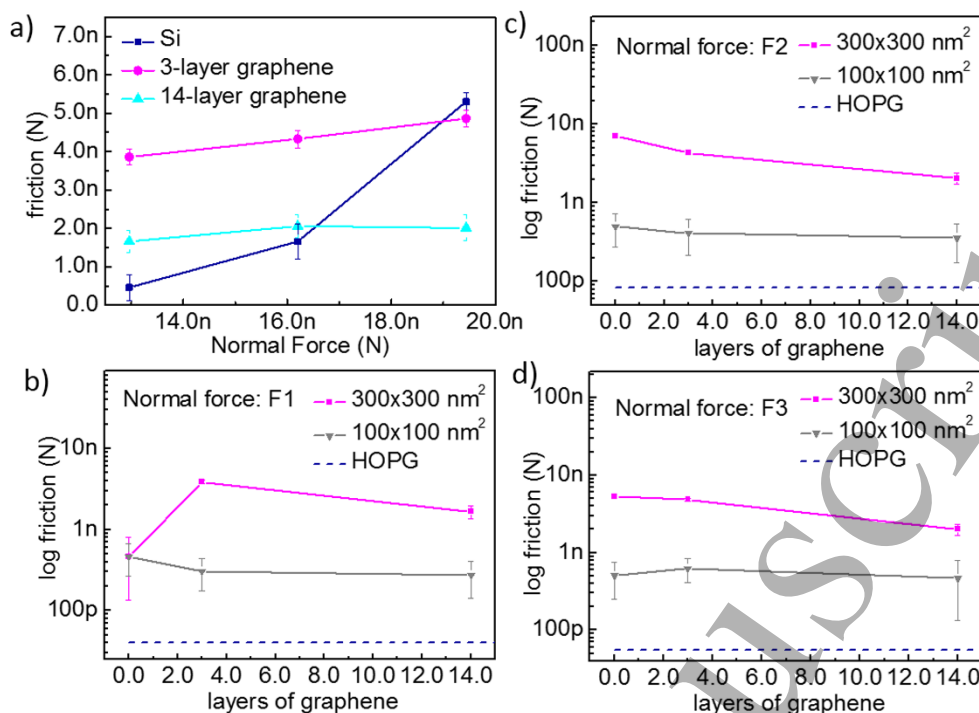
Figure 5. (a) The friction between AFM tip and sample surface as a function of applied normal forces in a (300 nm × 300 nm) region on surfaces of bare Si, 3-layer graphene on Si, and 14-layer graphene on Si. (b) – (d) The friction value (in log scale) obtained from both (300 nm × 300 nm) and (100 nm × 100 nm) scanning areas as a function of the graphene layers under a normal force (b) F1 = 12.96 nN, (c) F2 = 16.20 nN and (d) F3 = 19.44 nN.

Despite apparent reduction in both the friction and the frictional coefficient with increasing graphene layers as shown in figure 5(a), the lowest value of the frictional coefficient, 0.128 (= 1.66 nN/12.96 nN), still fell outside the range of superlubricity, because the measurements for figure 5(a) were carried out over areas that included steps of graphene layers. Noting that typical measurements of superlubricity generally excluded areas with defects or edges, we downsized the scan region to an atomically flat, (100 nm × 100 nm) area. Figure 5(b) shows the friction value (in log scale) as a function of the number of graphene layers measured from both (300 nm × 300 nm) and (100 nm × 100 nm) scan areas under the same load of F1 = 12.96 nN. For comparison, similar measurements were also conducted on a piece of highly oriented pyrolytic graphite (HOPG), which represented results obtained from a large number of graphene layers that approached infinity. The frictional coefficient of 0.0055 thus obtained from HOPG was consistent with a superlubricity surface, which further validated our experimental approach (see Experimental).

As illustrated in figure 5(b), the sliding friction exhibited a gradual decrease with increasing interfacial graphene layers for both scan areas. Moreover, friction obtained from the smaller area was more than one order of magnitude less than that obtained from the larger area, and the former reached an ultra-low frictional coefficient of ~ 0.015 (= 0.293 nN/19.44

nN), which was approaching the superlubricity (< 0.01) limit. To the best of our knowledge, this is the lowest measured frictional coefficient acquired between an AFM tip (with a radius ≤ 20 nm) and an as-grown graphene surface without using a lithographically fabricated graphite mesa as the sliding head. Similar experiments were also carried out under larger loads shown in figure 5(c) and 5(d) (with F2 = 16.20 nN, F3 = 19.44 nN). Both cases showed that surfaces with 14-layer graphene coverage displayed the lowest friction values when compared to those of either the bare Si surface or 3-layer graphene coverage. Furthermore, the trend of decreasing friction with increasing graphene layers for all loads of our study is expected to approach the superlubricity value of HOPG (dotted lines) when the number of graphene layers continues to increase. Our findings are consistent with recent theoretical calculations that demonstrate rapid damping of surface corrugations by misaligned layers of van der Waals materials [55]. Thus, our PECVD method for direct growth of multilayer graphene on Si provides a scalable approach to product ultra-low friction surfaces and further opens up a pathway towards significantly reducing friction on a wide variety of substrates by multilayers of van der Waals materials with a thickness larger than the penetration depth of the surface corrugation of substrates [57].

4. Conclusion and Outlook

In summary, we have demonstrated the feasibility of a single-step method for direct growth of large-area graphene and graphene-based nanomaterials on silicon by means of PECVD without active heating. By proper control of the PECVD growth parameters, we can obtain a variety of graphene-based materials, including large-area graphene sheets and vertically grown graphene nano-walls. Correlation between the growth parameters and the resulting sample characteristics has been made by studying the Raman spectroscopy, XPS, UPS, SEM, optical transmission and AFM, which helps unveil the growth mechanism and optimize the growth quality of graphene on silicon. RGA studies during the growth process suggests that a key factor for successful PECVD growth of graphene on Si is the revelation of surface Si dangling bonds by plasma-induced surface Si-O and Si-H bond-breaking, which enables efficient reaction of Si with carbon atoms disassociated from CH_4. Additionally, for Si substrates fully covered with multilayer graphene sheets, decreasing friction with increasing graphene layers has been demonstrated by AFM-based lateral force microscopy measurements. In particular, ultra-low friction with a load-independent frictional coefficient of ~ 0.015 has been achieved for an average of only ~ 14 layers of graphene on the Si surface. Thus, our demonstration of direct PECVD growth of large-area high-quality graphene on silicon suggests unprecedented opportunities for developing scalable and reproducible devices based on integrated graphene and silicon, which are not only promising for applications in areas of structural superlubricity but also for various silicon-based technologies such as optoelectronics and energy storage.

References

[1] Novoselov KS, Geim AK, Morozov SV, Jiang D, Katsnelson MI, Grigorieva IV, et al. Two-dimensional gas of massless Dirac fermions in graphene. *Nature*. 2005 **438** 197-200.

[2] Geim AK, Novoselov KS. The rise of graphene. *Nature Materials*. 2007 **6** 183-91.

[3] Miao F, Wijeratne S, Zhang Y, Coskun UC, Bao W, Lau CN. Phase-Coherent Transport in Graphene Quantum Billiards. *Science*. 2007 **317** 1530-3.

[4] Castro Neto AH, Guinea F, Peres NMR, Novoselov KS, Geim AK. The electronic properties of graphene. *Rev Mod Phys*. 2009 **81** 109-62.

[5] Xu H, Ma L, Jin Z. Nitrogen-doped graphene: Synthesis, characterizations and energy applications. *Journal of Energy Chemistry*. 2018 **27** 146-60.

[6] Berman D, Erdemir A, Sumant AV. Graphene: a new emerging lubricant. *Materials Today*. 2014 **17** 31-42.

[7] Holmberg K, Andersson P, Erdemir A. Global energy consumption due to friction in passenger cars. *Tribology International*. 2012 **47** 221-34.

[8] Cao S, Wang J, Ding Y, Sun M, Ma F. Visualization of weak interactions between quantum dot and graphene in hybrid materials. *Scientific Reports*. 2017 **7** 417.

[9] Lee C, Wei X, Kysar JW, Hone J. Measurement of the Elastic Properties and Intrinsic Strength of Monolayer Graphene. *Science*. 2008 **321** 385-8.

[10] Sokoloff JB. Effects of defects on the friction between film and substrate in a microbalance experiment. *Physical Review B*. 1995 **51** 15573-4.

[11] van Wijk MM, Dienwiebel M, Frenken JWM, Fasolino A. Superlubric to stick-slip sliding of incommensurate graphene flakes on graphite. *Physical Review B*. 2013 **88** 235423.

[12] Zheng Q, Jiang B, Liu S, Weng Y, Lu L, Xue Q, et al. Self-Retracting Motion of Graphite Microflakes. *Physical Review Letters*. 2008 **100** 067205.

[13] Liu Z, Yang J, Grey F, Liu JZ, Liu Y, Wang Y, et al. Observation of Microscale Superlubricity in Graphite. *Physical Review Letters*. 2012 **108** 205503.

[14] Li R, Li Z, Pambou E, Gutfreund P, Waigh TA, Webster JRP, et al. Determination of PMMA Residues on a Chemical-Vapor-Deposited Monolayer of Graphene by Neutron Reflection and Atomic Force Microscopy. *Langmuir*. 2018 **34** 1827-33.

[15] Liang X, Sperling BA, Calizo I, Cheng G, Hacker CA, Zhang Q, *et al.* Toward Clean and Crackless Transfer of Graphene. *ACS Nano*. 2011 **5** 9144-53.

[16] Jin Z, McNicholas TP, Shih CJ, Wang QH, Paulus GLC, Hilmer AJ, *et al.* Click Chemistry on Solution-Dispersed Graphene and Monolayer CVD Graphene. *Chemistry of Materials*. 2011 **23** 3362-70.

[17] Jin Z, Yao J, Kittrell C, Your JM. Large-Scale Growth and Characterizations of Nitrogen-Doped Monolayer Graphene Sheets. *ACS Nano*. 2011 **5** 4112-17.

[18] Leong WS, Wang H, Yeo J, Martin-Martinez FJ, Zubair A, Shen P-C, *et al.* Paraffin-enabled graphene transfer. *Nature Communications*. 2019 **10** 867.

[19] Gao L, Ren W, Xu H, Jin L, Wang Z, Ma T, *et al.* Repeated growth and bubbling transfer of graphene with millimetre-size

single-crystal grains using platinum. *Nature Communications*. 2012 **3** 699.

[20] Lin W-H, Chen T-H, Chang J-K, Taur J-I, Lo Y-Y, Lee W-L, *et al.* A Direct and Polymer-Free Method for Transferring Graphene Grown by Chemical Vapor Deposition to Any Substrate. *ACS Nano*. 2014 **8** 1784-91.

[21] Jin Z, Lomeda JR, Price BK, Lu W, Zhu Y, Tour JM. Mechanically Assisted Exfoliation and Functionalization of Thermally Converted Graphene Sheets. *Chemistry of Materials*. 2009 **21** 3045-47.

[22] Liu P, Jin Z, Katsukis G, Drahushuk LW, Shimizu S, Shih CJ, *et at*. Layered and scrolled nanocomposites with aligned semi-infinite graphene inclusions at the platelet limit. Science. 2016 **353** 364-7.

[23] Phare CT, Lee YHD, J. Cardenas J, Lipson M. Graphene electro-optic modulator with 30 GHz bandwidth. *Nature Photonics*. 2015 **9** 511–4.

[24] Huidobro PA, Kraft M, Maier SA, Pendry JB. Graphene as a tunable anisotropic or isotropic plasmonic metasurface,. *ACS Nano*. 2016 **10** 5499–506.

[25] Casalino M *et al.* Vertically illuminated, resonant cavity enhanced, graphene-silicon Schottky photodetectors. *ACS Nano*. 2017 **11** 10955–963.

[26] Chang P *et al.* Highly sensitive graphene − semiconducting polymer hybrid photodetectors with millisecond response time. *ACS Photonics*. 2017 **4** 2335-44

[27] Levy U, Grajower M, Gonçalves PAD, Mortensen NA, Khurgin JB. Plasmonic silicon Schottky photodetectors: The physics behind graphene enhanced internal photoemission. *APL Photonics*. 2017 **2** 026103.

[28] Gan S, Zhang Y, Bao Q. Graphene-based optical modulators. *Graphene Photonics, Optoelectron. Plasmon.* 2017 41–56.

[29] Limmer T. Influence of carrier density on the ultrafast optical response of graphene and few-layer graphene. 2012 PhD dissertation, der Ludwig-Maximilians-Universität München.

[30] Hwang J, Kim M, Campbell D, Alsalman HA, Kwak JY, Shivaraman S, et al. van der Waals epitaxial growth of graphene on sapphire by chemical vapor deposition without a metal catalyst. *ACS Nano*. 2013 **7** 385-95.

[31] Tai L, Zhu D, Liu X, Yang T, Wang L, Wang R, et al. Direct growth of graphene on silicon by metal-free chemical vapor deposition. *Nanomicro Lett*. 2018 **10** 20.

[32] Trung PT, Joucken F, Campos-Delgado J, Raskin J-P, Hackens B, Sporken R. Direct growth of graphitic carbon on Si(111). *Applied Physics Letters*. 2013 **102** 013118.

[33] Hong G, Wu Q-H, Ren J, Lee S-T. Mechanism of non-metal catalytic growth of graphene on silicon. *Applied Physics Letters*. 2012 **100** 231604.

[34] Hod O, Meyer E, Zheng Q, Urbakh M. Structural superlubricity and ultralow friction across the length scales. *Nature*. 2018 **563** 485-92.

[35] Liu M, Yin X, Ulin-Avila E, Geng B, Zentgraf T, Ju L, et al. A graphene-based broadband optical modulator. *Nature*. 2011 **474** 64-7.

[36] Sorianello V, Midrio M, Romagnoli M. Design optimization of single and double layer Graphene phase modulators in SOI. *Opt Express*. 2015 **23** 6478-90.

[37] Montanaro A, Mzali S, Mazellier J-P, Bezencenet O, Larat C, Molin S, et al. Thirty Gigahertz Optoelectronic Mixing in

Chemical Vapor Deposited Graphene. *Nano Letters*. 2016 **16** 2988-93.

[38] Kim K, Choi J-Y, Kim T, Cho S-H, Chung H-J. A role for graphene in silicon-based semiconductor devices. *Nature*. 2011 **479** 338-44.

[39] Mao D, Kananen T, Li T, Soman A, Sinsky J, Petrone N, et al. Bandwidth Limitation of Directly Contacted Graphene–Silicon Optoelectronics. *ACS Applied Electronic Materials*. 2019 **1** 172-8.

[40] Ooi KJA, Leong PC, Ang LK, Tan DTH. All-optical control on a graphene-on-silicon waveguide modulator. *Scientific Reports*. 2017 **7** 12748.

[41] Donnelly C, Tan DTH. Ultra-large nonlinear parameter in graphene-silicon waveguide structures. *Opt Express*. 2014 **22** 22820-30.

[42] Ooi KJA, Chu HS, Ang LK, Bai P. Mid-infrared active graphene nanoribbon plasmonic waveguide devices. *J Opt Soc Am B*. 2013 **30** 3111-6.

[43] Chemical Industry Digest. Graphene silicon combo could be next gen lithium ion batteries n.d. [Available from: https://chemindigest.com/graphene-silicon-combo-could-be-next-gen-lithium-ion-batteries/?fbclid=IwAR2uZi7jhGuGoriuN0MUHWaP_gFwBZpnF6MXkHyYULUeqIhnvJ8TNzriXlE.

[44] Chabot V, Feng K, Park HW, Hassan FM, Elsayed AR, Yu A, et al. Graphene wrapped silicon nanocomposites for enhanced electrochemical performance in lithium ion batteries. *Electrochimica Acta*. 2014 **130** 127-34.

[45] Zhao G, Zhang L, Meng Y, Zhang N, Sun K. Decoration of graphene with silicon nanoparticles by covalent immobilization for use as anodes in high stability lithium ion batteries. *Journal of Power Sources*. 2013 **240** 212-8.

[46] Han C-P, Veeramani V, Hsu C-C, Jena A, Chang H, Yeh N-C, et al. Vertically-aligned graphene nanowalls grown via plasma-enhanced chemical vapor deposition as a binder-free cathode in Li–O_2 batteries. *Nanotechnology*. 2018 **29** 505401.

[47] Lin L-Y, Kim D-E, Kim W-K, Jun S-C. Friction and wear characteristics of multi-layer graphene films investigated by atomic force microscopy. Surface and Coatings Technology. 2011 205 4864-9.

[48] Yeh NC, Hsu CC, Bagley J, Tseng WS. Single-step growth of graphene and graphene-based nanostructures by plasma-enhanced chemical vapor deposition. *Nanotechnology*. 2019 **30** 162001.

[49] Boyd DA, Lin WH, Hsu CC, Teague ML, Chen CC, Lo YY, et al. Single-step deposition of high-mobility graphene at reduced temperatures. *Nat Commun*. 2015 **6** 6620.

[50] Malard LM, Pimenta MA, Dresselhaus G, Dresselhaus MS. Raman spectroscopy in graphene. *Physics Reports*. 2009 **473** 51-87.

[51] Wu J-B, Lin M-L, Cong X, Liu H-N, Tan P-H. Raman spectroscopy of graphene-based materials and its applications in related devices. *Chemical Society Reviews*. 2018 **47** 1822-73.

[52] Shearer CJ, Slattery AD, Stapleton AJ, Shapter JG, Gibson CT. Accurate thickness measurement of graphene. *Nanotechnology*. 2016 **27** 125704.

[53] Nemes-Incze P, Osváth Z, Kamarás K, Biró LP. Anomalies in thickness measurements of graphene and few layer graphite

crystals by tapping mode atomic force microscopy. *Carbon*. 2008 **46** 1435-42.

[54] Basov DN, Fogler MM, García de Abajo FJ. Polaritons in van der Waals materials. *Science*. 2016 **354** aag1992.

[55] Hsu C-C, Bagley JD, Teague ML, Tseng W-S, Yang KL, Zhang Y, et al. High-yield single-step catalytic growth of graphene nanostripes by plasma enhanced chemical vapor deposition. *Carbon*. 2018 **129** 527-36.

[56] Nair RR, Blake P, Grigorenko AN, Novoselov KS, Booth TJ, Stauber T, et al. Fine Structure Constant Defines Visual Transparency of Graphene. *Science*. 2008 **320** 1308.

[57] Mandelli D, Ouyang W, Urbakh M, Hod O. The Princess and the Nanoscale Pea: Long-Range Penetration of Surface Distortions into Layered Materials Stacks. *ACS Nano*. 2019 **13** 7603-9.